Control of a Flywheel Energy Storage System for Power Smoothing in Wind Power Plants

Francisco Díaz-González, *Student Member, IEEE,* Fernando D. Bianchi, Andreas Sumper, *Member, IEEE,* Oriol Gomis-Bellmunt, *Senior Member, IEEE*

***Abstract*—This work deals with the design and the experimental validation in scale-lab test benches of an energy management algorithm based on feedback control techniques for a flywheel energy storage device. The aim of the flywheel is to smooth the net power injected to the grid by a wind turbine or by a wind power plant. In particular, the objective is to compensate the power disturbances produced by the cycling torque disturbances of the wind turbines due to the airflow deviation through its tower section. The article describes the control design, its tuning, as well as the description of the experimental setup and the methods for the experimental validation of the proposed concepts. Results show that the fast wind power fluctuations can be mostly compensated through the flywheel support.**

***Index Terms*—Power smoothing, feedback control, flywheel, energy storage, wind turbines**

I. Introduction

THE variability of wind power could markedly affect power quality in, especially, weak or isolated grids [1], [2], [3], [4], [5], [6]. For instance, high flicker levels can be provoked by periodic fluctuations to the torque of the turbine and other stochastic factors related to the randomness of wind. To minimize the effects of the variability of wind power, an energy storage system can be used [7], [8], [9]. Furthermore, the utilization of energy storage devices together with wind turbines have some additional functionalities, such as frequency support and matching of forecasted and real active power production. The most suitable energy storage technologies for smoothing the fast fluctuations of the power generated by the wind turbines are those with high ramp power rates and high cycling capability. In this regard, storage technologies such as supercapacitors, superconducting magnetic energy storage devices and flywheel energy storage systems (FESS) are well suited.

Flywheel stores kinetic energy in a high-speed rotational disk coupled to the shaft of an electric machine [10], [11], [12], [13]. The storage device is charged when the machine operates as a motor (the flywheel accelerates). Conversely, the device is discharged when the machine regenerates through the drive (slowing the flywheel). The energy stored depends on the product of the square of the rotational speed and the inertia. The use of optimized electrical machines, vacuum systems to reduce wind shear and magnetic bearings to reduce friction losses among other components favours the high efficiency of flywheels (around 90% at rated power), long cycling life and high power and energy densities [12], [11], [8]. Among the major drawbacks of the technology, the high standing losses are remarkable, as lead self discharge rates of about 20% of the stored capacity per hour [14]. For this reason, flywheels are not suitable for long-term energy storage.

Flywheel systems are effective for wind power smoothing. Related studies address two control levels: the design of high-level energy management algorithms of the storage device and the research in the low-level control scheme of the electrical machine.

The term low-level control scheme refers to the control system that manages the instantaneous electrical currents through the flywheel so that it can consume or inject the required electrical power. It is, therefore, a problem framed in the field of the control of electrical machines. In this sense, it is worth noting that control schemes of permanent magnet synchronous machines, squirrel cage machines [15], [16], [17] and switched reluctance machines [18] are addressed. Research focuses on developing field weakening strategies to enable the electrical machine to rotate above the rated speed and thus, to maximize the energy capacity of the storage device. Also, other aspects like the research in sensorless control techniques and also in the topology of the power electronics to drive the electrical machine are considered.

In contrast, the term high-level energy management algorithm refers to a supervisor, which aim is to maintain the State of Charge (SoC) of the flywheel within certain operating limits. This algorithm determines the set points to the low-level control scheme of the electrical machine of the flywheel, i.e. the instantaneous torque (or power) reference. The inputs to this algorithm are usually the power of the wind turbine and the measurement of the SoC of the storage device. The supervision of the SoC ensures the availability of the flywheel for compensating the wind power fluctuations when required. Within the related studies, several proposals based on fuzzy-logic schemes can be found [20], [21], [22]. Despite the fact that the SoC is maintained within certain operating limits in the previous works, its average value is not controlled. However,

F. Díaz-González is with Catalonia Institute for Energy Research (IREC), C. Jardins de les Dones de Negre, 1, Pl. 2a, 08930 Sant Adrià del Besòs, Spain (e-mail: fdiazg@irec.cat).

F. D. Bianchi is with Catalonia Institute for Energy Research (IREC) (e-mail: fbianchi@irec.cat).

A. Sumper is with Catalonia Institute for Energy Research (IREC) and also with Centre d'Innovació Tecnològica en Convertidors Estàtics i Accionaments (CITCEA-UPC), Departament d'Enginyeria Elèctrica, Universitat Politècnica de Catalunya EU d'Enginyeria Tècnica Industrial de Barcelona, C. Comte d'Urgell, 187, Pl. 2, 08036 Barcelona, Spain (e-mail: sumper@citcea.upc.edu).

O. Gomis-Bellmunt is with Catalonia Institute for Energy Research (IREC) and also with Centre d'Innovació Tecnològica en Convertidors Estàtics i Accionaments (CITCEA-UPC), (e-mail: gomis@citcea.upc.edu).

in [26] it has been concluded that an improvement in the power smoothing can be achieved if the average SoC is adjusted with respect to the expected energy to be exchanged between the network and the storage device.

This paper proposes a novel high-level control algorithm of a flywheel-based storage device using the expected energy exchanged to maintain an optimal SoC and thus to improve the smoothing of the power injected by a wind turbine or by a wind power plant. The high-level control algorithm is in charge of managing the energy stored in the flywheel so that it can compensate as much as possible the turbulent components of the wind power. The aim of the control algorithm is to maintain a determined average SoC, i.e. an average rotational speed of the flywheel, while also permitting the fast accelerations and decelerations of the machine for compensating the turbulent components of the wind power. Similarly to [19], [20], [21], [22], the high-level control algorithm determines the set points to the low-level one from the measurement of the rotational speed of the flywheel and the wind power. As a difference with the above mentioned works, the proposal of the present article is based on active power control through an I-P control structure [23], [24] instead of fuzzy-logic-based control schemes. The proposed control scheme has been evaluated experimentally in laboratory. The main advantages with respect to previous works based on fuzzy-logic are design procedure, ensuring specific dynamic performance, and the simplicity of the proposed algorithm. The latter is an important point since the computation time in these schemes could be a constraint for their implementation in industrial computers [21].

II. Wind power smoothing by flywheels

The power generated by the wind turbines depends on deterministic and stochastic factors related to the variability of the wind. Among the deterministic factors the wind shear and the presence of other turbines and obstacles can be noted. Among the stochastic factors, it is worth highlighting the wind turbulence and the rotating sampling effect. All these factors affect the power generated by the wind turbines in the time range of seconds [4], [25].

While the effect of wind shear is alleviated from the summation torque of the blades, the rotating sampling effect leads noticeable cycling torque disturbances due to the airflow deviation through the tower section. The product of the mean rotational speed of the turbine P and the number of blades determines the frequency of this disturbance. The power spectrum produced by a typical 3 bladed wind turbine can be observed in Figure 1 (which is deeply described in [26]).

The wind model and the model of the variable speed wind turbine which lead the power spectrum in Figure 1 are explained in previous work of the authors of the present article [26].

The present work focuses on the smoothing of the turbulent components of the power which mainly correspond to the rotating sampling effect. Only partial load operation of the wind turbines is considered, as the variability of the power generated is alleviated from the action of the pitch actuator in the full load operating region of the turbines.

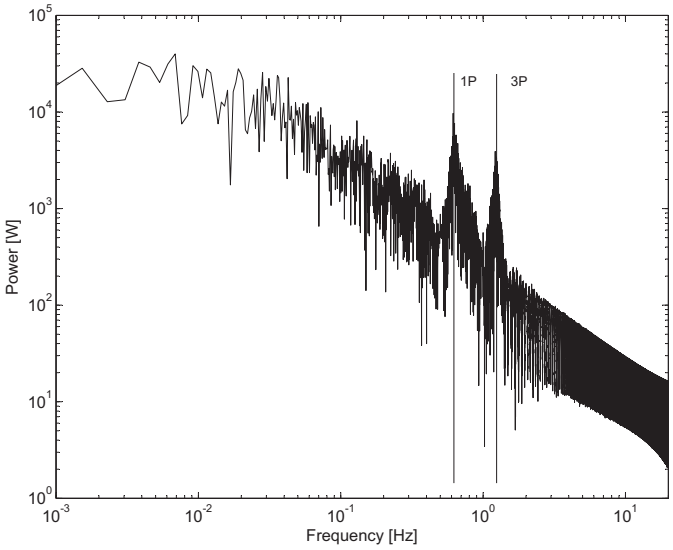

Fig. 1. Power spectrum of a three blade wind turbine of 1.5 MW. Mean wind speed is 7 m/s.

To smooth the net power injection to the grid, the flywheel is added to the point of connection of the wind turbine. The flywheel is in charge of fastly injecting and absorbing power so that it can compensate the wind power fluctuations. The turbulent components of the wind power to be compensated are obtained from filtering the wind power measurement P_{wt}. This power filtering is part of the flywheel control system which receives also the measurement of the flywheel speed ω_{fw}. From these signals the high-level control algorithm sets out the electrical torque reference T^*_{fw} for the machine side converter of the flywheel, so that the net power injection by the flywheel and the wind turbine becomes smoothed as much as possible. The proposed control scheme is detailed in Figure 2.

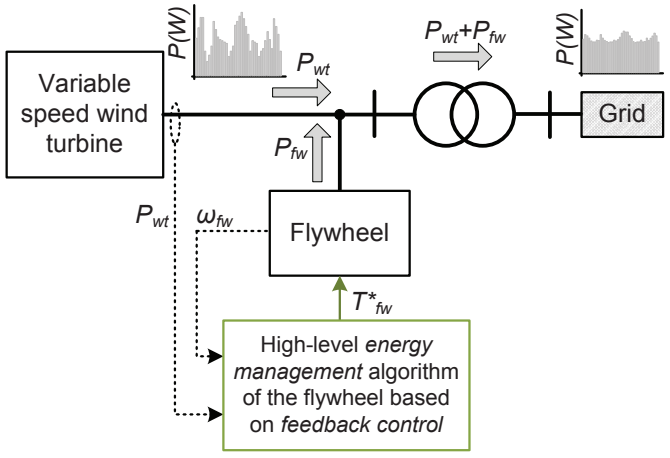

Fig. 2. Conceptual diagram of the proposed control scheme.

The electrical torque reference T^*_{fw} set by the energy management algorithm of the flywheel permits the storage device to accelerate and brake but also to maintain a determined average SoC within the specified operating limits.

In [26], it is found that in order to operate the flywheel in an optimal way, i.e. to smooth as much as possible the turbulent components of the wind turbine, the storage device has to maintain a determined average rotational speed function of the average power generated by the wind turbine. This is motivated from the dependence between the power capacity of the flywheel and its rotational speed. In fact, the power that the flywheel is capable of exchanging results from the product of its rotational speed and its rated torque. Moreover, the magnitude of the turbulent components of wind power to be compensated by the flywheel depends on the power generated by the turbine which is greater in high wind speeds.

Accordingly, it is proposed to adjust the average SoC of the flywheel with the average power generated by the wind turbine to fit the power capacity of the flywheel to the expected wind power to be compensated.

Also, the inclusion of an energy management algorithm of the flywheel is motivated from the following reasons:

1) The limited energy capacity of the flywheel. Without an energy management strategy, the storage device would frequently become fully charged or discharged, thus limiting its operability.
2) The need of compensating the high-standing losses of the flywheel. Compensating the turbulent components of the wind power requires the flywheel to exchange a power series with average value close to zero. However, without a proper compensation of the standing losses, the storage device will become continuously discharged.
3) The possibility of reducing the losses of the flywheel in operation. The losses of the flywheel increase with the rotational speed. Thus, there is no reason to concern, for instance, high average rotational speeds if the flywheel is intended of just exchanging low levels of power.

Following sections describe the design of the energy management algorithm of the flywheel.

III. Design of the high-level energy management algorithm of the flywheel

The energy management algorithm of the flywheel is presented in Figure 3. As can be noted, the algorithm consists of two main parts: the so-called inputs filtering and processing; and the feedback control. These two parts are described in the next subsections.

A. Inputs filtering and processing

As described in Section II, the high-level energy management algorithm of the flywheel has two main objectives: to let the flywheel maintain an optimum average rotational speed while enabling the fast accelerations and decelerations of the system. Mathematically, achieving these two objectives means to track the average rotational speed reference $\bar{\omega}^*_{fw}$ and the high frequency torque reference d^*. These signals are the setpoints enter the feedback control in different point as can be seen in Figure 3. The block "inputs filtering and processing" in the energy management algorithm computes these setpoint signals from the input signals ω_{fw} and P_{wt}.

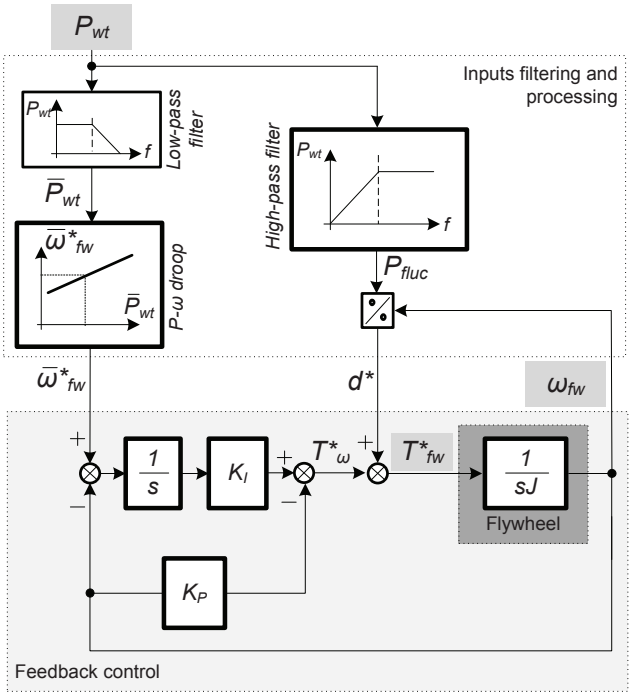

Fig. 3. Energy management algorithm of the flywheel. The input signals of the algorithm (P_{wt} and ω_{fw}) as well as the output T^*_{fw} are shaded in grey.

The optimum average rotational speed reference $\bar{\omega}^*_{fw}$ depends on the mean wind power (with averaging period several minutes) and is obtained from solving an optimization problem presented in [26]. This optimization problem is a mixed integer non linear problem solved in GAMS software. The problem takes a time series of the fluctuating components of wind power to be compensated by the flywheel and tries to minimize the difference between this and the instantaneous power exchanged by the flywheel, taking also into account the losses of the storage device. As a result, a corresponding time series of the optimal instantaneous flywheel speed, i.e. the optimal instantaneous SoC, is obtained. The problem is solved for sufficient representative cases (two hundred) in which several time series of wind power are considered. Then, the analysis of the obtained results, leads an almost linear relation between the mean wind power and the flywheel optimum average rotational speed reference $\bar{\omega}^*_{fw}$. That is why, in the present paper, the dependency between these two variables is represented by the $P-\omega$ droop characteristic (see Figure 3).

While the optimum average rotational speed reference $\bar{\omega}^*_{fw}$ is a slowly varying signal, the torque reference d^* contents high frequency components. The reference d^* is computed from

$$d^* = \frac{P_{fluc}}{\omega_{fw}}, \tag{1}$$

where P_{fluc} corresponds to the fast wind power fluctuations that must be attenuated. This signal is obtained from passing the wind power measures through a high pass filter. The cutoff frequency of this filter is chosen so that the power disturbances caused by the rotating sampling effect passes through the filter without significant distortion.

B. Feedback control

The aim of the feedback control is to ensure the tracking of the slowly varying reference $\bar{\omega}^*_{fw}$ and the fast varying reference d^*. To this end, an I-P controller acts on the torque reference T^*_ω to regulate the instantaneous rotational speed of the flywheel ω_{fw}. The I-P structure facilitates the development of a systematic procedure for the tuning of the controller. Also, it satisfies the two first motivations (or control requirements) for the energy management algorithm that are depicted in Section II. As a reminder, the first and the second requirement refer to the need of not overcoming the operating limits of the storage device, and of compensating the standing losses of the flywheel. These requirements are satisfied by the proportional and integral parts of the controller. The third requirement of the energy management algorithm refers to the need of varying the average SoC with the average wind power. This is satisfied by adding the previously presented $P-\omega$ droop characteristic (see Figure 3).

As can be seen in Figure 3, the torque reference T^*_{fw} is the sum of the torque d^* and the compensation term

$$T^*_w = K_I \int (\bar{\omega}^*_{fw} - \omega_{fw})dt - K_P \omega_{fw}. \tag{2}$$

The parameters K_I and K_P of the I-P controller are tuned to shape the frequency responses of the transfer functions from $\bar{\omega}^*_{fw}$ to ω_{fw} and from d^* to ω_{fw}.

Note that the error between the reference signal and the feedback of the plant is affected by a pure integrator in both P-I and I-P controllers. However, as a difference with conventional P-I controllers, in I-P controllers the proportional gain does not affect the error signal but the feedback of the plant instead (Figure 3).

For the controller design purpose, the plant (the flywheel) is characterized by its mechanical dynamics imposed by the inertia J (see Figure 3). The fast electrical dynamics of the machine is omitted as being much faster than the mechanical one. Accordingly, the flywheel speed is given by

$$\omega_{fw}(s) = \frac{1}{Js + K_P}\left(d^*(s) + \frac{K_I}{s}(\bar{\omega}^*_{fw}(s) - \omega_{fw}(s))\right). \tag{3}$$

Then, reorganizing terms

$$\omega_{fw}(s) = T_{d^*\omega}(s)d^*(s) + T(s)\bar{\omega}^*_{fw}, \tag{4}$$

where

$$T_{d^*\omega}(s) = \frac{s}{Js^2 + K_P s + K_I}, \tag{5}$$

$$T(s) = \frac{K_I}{Js^2 + K_P s + K_I}. \tag{6}$$

The reference d^* is not a completely exogenous signal since it depends on the flywheel speed according to (1). To consider this fact in the parameter tuning and guarantee stability in all possible values of power and flywheel speed, the reference is expressed as

$$d^* = \delta \cdot \omega_{fw}, \tag{7}$$

where $\delta = P_{fluc}/\omega^2_{fw}$ is a time varying parameter taking values in the interval $[-\delta_{max}, \delta_{max}]$ with

$$\delta_{max} = \frac{P^*_{max}}{\omega^2_{min}}. \tag{8}$$

With the previous definitions and using the small gain theorem [32], it is possible to state conditions to ensure stability of the close loop systems for all acceptable values of power and rotational speed. More precisely, the closed loop system is stable for all values of δ in $[-\delta_{max}, \delta_{max}]$ if the infinite norm of the transfer function from d^* to the output of the plant ω_{fw} ($T_{d^*\omega}$) does not exceed the upper limit δ_{max}, i.e.

$$||T_{d^*\omega}||_\infty = \max_\omega |T_{d^*\omega}(j\omega)| < \delta_{max}. \tag{9}$$

Assuming that the transfer function $T_{d^*\omega}$ has two real and different poles, i.e.

$$\begin{aligned} T_{d^*\omega} &= \frac{s/K_I}{(s/p_1 + 1)(s/p_2 + 1)} \\ &= \frac{s/K_I}{\frac{1}{p_1 p_2}s^2 + \left(\frac{1}{p_1} + \frac{1}{p_2}\right)s + 1}. \end{aligned} \tag{10}$$

If p_1 is the dominant pole ($p_1 \ll p_2$), then

$$||T_{d^*\omega}||_\infty < \frac{p_1}{K_I} < \frac{1}{\delta_{max}}. \tag{11}$$

Therefore, the integrator gain K_I should satisfy

$$K_I > p_1 \delta_{max} \tag{12}$$

to ensure closed loop stability for all possible values of power and speed. Further, the proportional gain can be obtained from comparing the denominators of (5) and (10),

$$K_P = K_I\left(\frac{1}{p_1} + \frac{1}{p_2}\right), \tag{13}$$

where $p_2 = K_I/Jp_1$.

In Figure 4, an asymptotic graph of the frequency responses of $T_{d^*\omega}$ and T can be observed. The pole p_1 defines the bandwidth of the speed tracking as well as the infinity norm of $T_{d^*\omega}$. Therefore, once the bandwidth of T, the parameters of the controller can be computed from (12) and (13).

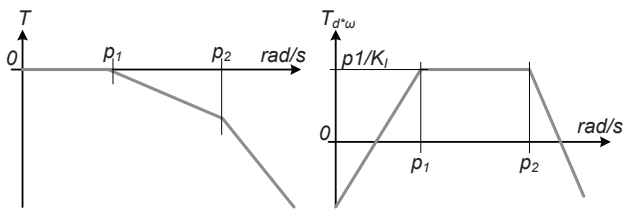

Fig. 4. Asymptotic diagram of the frequency responses of the transfer functions $T_{d^*\omega}$ and T.

IV. Experimental validation

This section describes the flywheel test bench, the wind turbine emulator as well as the rest of the laboratory equipment used for configuring the system for the purposes of the study. Emphasis is done in presenting those actions needed to emulate the variability of the power of the wind turbine in a lab-scaled equipment among other considerations. Then, experimental results are analysed with the aim of validating the proposed energy management algorithm of the flywheel.

A. Description of the experimental setup

Figure 5 presents an scheme of the experimental setup. As can be noted, the system is composed by a flywheel test bench, a wind turbine emulator, a coupling transformer which connects the system to the grid, measurement devices and communication and control devices. Each of these main components of the system are detailed as follows.

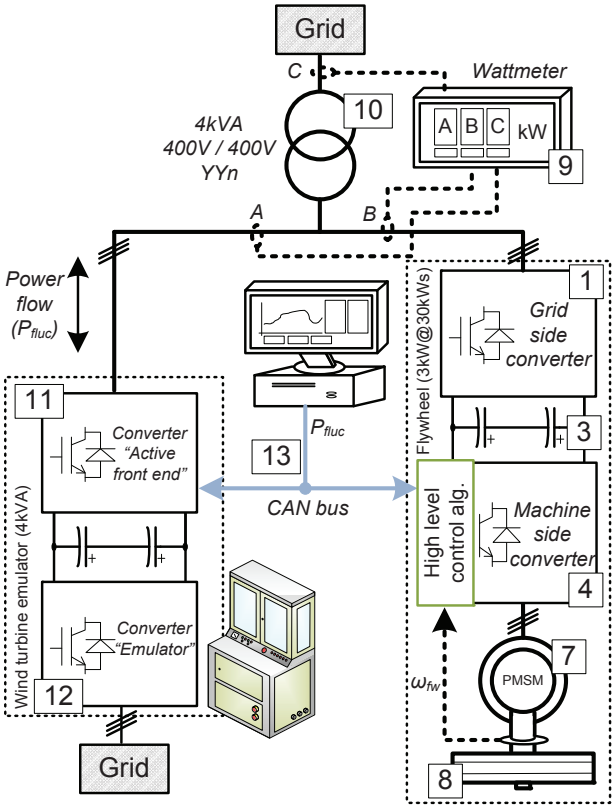

Fig. 5. Scheme of the experimental setup.

1) Flywheel test bench: Figure 6 shows the flywheel test bench. The system is composed by a rotating disk mechanically coupled to the shaft of a permanent magnet synchronous machine (PMSM). The electrical machine is controlled by a set of back-to-back power converters. These power converters are driven by digital signal processor (DSP)-based control boards.

As previously noted, the flywheel is added to the point of connection of the wind turbine emulator. The design and experimental validation of the low-level algorithm of the power converters of the flywheel test bench are deeply explained in [27]. As a summary, the grid side converter of the system is in charge of regulating the voltage of the dc link of the back-to-back power converters and also the reactive currents exchanged with the network. The control of the machine side converter is the field oriented vector control system of the PMSM [29], [30]. This control algorithm governs the PMSM so that it follows the instantaneous electrical torque T^*_{fw} referenced by the energy management algorithm.

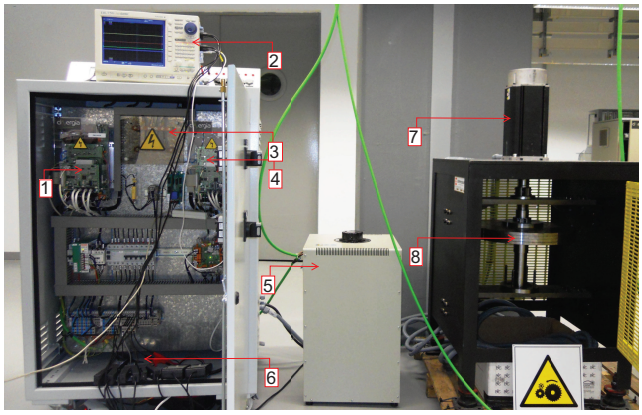

Fig. 6. Flywheel test bench. From left to right: 1) grid side conv.; 2) oscilloscope; 3) dc link; 4) machine side conv.; 5) autotransformer; 6) measurement devices; 7) PMSM; 8) rotating disk.

The rated power capacity of the storage device is 3 kW, and the energy capacity is 30 kWs. Further parameters of the system are presented in Table I in Appendix.

2) Wind turbine emulator: The wind turbine is emulated by a cabinet composed by two identical three phase voltage sources in back-to-back configuration [28] (see Figure 5).

A bidirectional power flow through the converters is possible since they can be operated as either active rectifiers or active inverters. According to Figure 5, power flows from the ac side of the converter "emulator" to the ac side of the converter "active front end" while representing the behaviour of a generator. The reverse process depicts the behaviour of a load. The low-level control algorithms of the power converters of the cabinet receive the series of active and reactive power set points to represent the power profile of the wind turbine. The rated apparent power of the cabinet is bounded to 4 kVA. The relevant parameters of the cabinet for the purposes of the present article are presented in Table I in Appendix. Further details of the cabinet are presented in [28].

3) Measurement devices: For the purposes of the work, it is needed to analyze the variability of the power injected by the emulator of the wind turbine, and its attenuation from the inclusion of the flywheel. Accordingly, a wattmeter registers simultaneously the power series in the points A, B and C depicted in Figure 5 for their post processing and analysis. These points corresponds to the terminals of the wind turbine emulator, the terminals of the flywheel test bench, and the point of connection of the system to the network respectively. Figure 7 depicts the wattmeter, the coupling transformer for the connection of the system to the network and the wind turbine emulator.

4) Communications: As presented in Figure 5, the wind turbine emulator represents the variability of the power of the

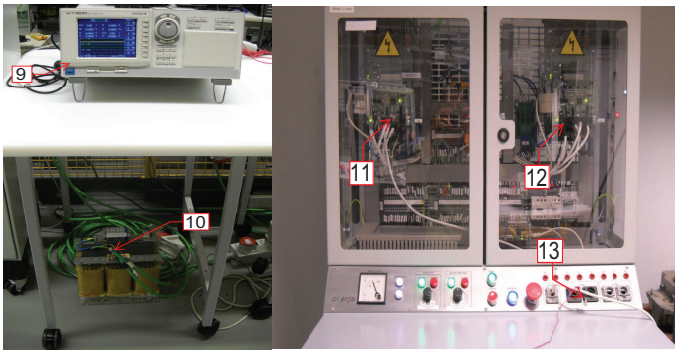

Fig. 7. Experimental setup. From left to right: 9) wattmeter; 10) coupling transformer; 11) power converter of the wind turbine emulator "active front end"; 12) power converter "emulator"; 13) CAN bus port.

wind turbine following the power set-points sent through a Controller Area Network (CAN) bus by a computer. CAN bus is also used to let the energy management algorithm of the flywheel know the above mentioned wind power. The precise clocking of the digital signal processor (DSP) of the control board the machine side power converter of the flywheel is used as a time basis to coordinate the exchange of signals between the computer, the wind turbine emulator and the flywheel. In particular, the signals are sent through the CAN bus each 20 milliseconds.

B. Assumptions for the emulation of the fluctuating components of wind power

According to Figure 3, the average optimum rotational speed of the flywheel $\bar{\omega}^*_{fw}$ and also the wind power fluctuations P_{fluc} have to be determined from filtering the generated power by a wind turbine P_{wt}. However, the presented experimental validation avoids the emulation of the power P_{wt} and consequently its filtering. Only the wind power fluctuation P_{fluc} is actually emulated instead by the wind turbine emulator. Thus, P_{fluc} is a power profile with average value close to zero that is obtained from the simulation of the system and the application of the high-pass filter to the output of the model of the wind turbine P_{wt}.

This is carried out with the aim of adjusting the magnitude of the wind power fluctuations P_{fluc} to the actual power ratings of the flywheel test bench and the wind turbine emulator. The present work considers a scaling factor of 20 for the power of a 1.5 MW wind turbine. The magnitude of the resultant profile P_{fluc} is similar to the ratings of the wind turbine emulator (4 kVA), and also to the ratings of the flywheel test bench (3 kW). Therefore, the size of the flywheel test bench can be considered adequate to compensate the fluctuations of the power of a wind turbine with a rated power 1.5/20 MW.

Figure 8 plots the results of the simulation of a 1.5 MW wind turbine. Its power output profile P_{wt} has been scaled by a factor of 20. The subplot below shows the resultant P_{fluc}. As can be noted, the magnitude of P_{fluc} is bounded to 3 kW approximately, which corresponds to the rated power of the flywheel test bench. The cutoff frequency of the high pass filter of P_{wt} is set to 0.4 Hz so that the rotating sampling effect can be represented. The details of this filter can be found in Appendix.

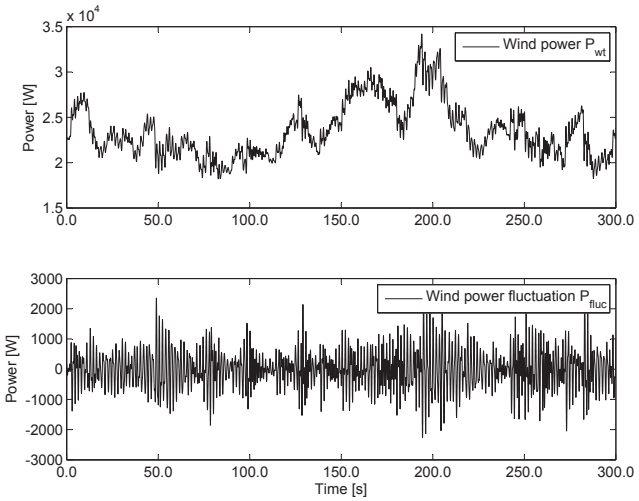

Fig. 8. Scaled magnitude of the power output of a 1.5 MW wind turbine and the fluctuating components of it from a cutoff frequency of 0.4 Hz.

As a consequence of the direct emulation of P_{fluc}, the $P-\omega$ droop characteristic (Figure 3) is not applied. Therefore, the optimum average rotational speed of the flywheel $\bar{\omega}^*_{fw}$ will be step-profiled in following sections for evaluating the performance of the designed feedback control.

C. Determination of the control parameters for the experimental system

Section III-B depicts the procedure for the tuning of the parameters of the I-P structure which builds up the feedback control. The present section presents the particular values of the controller determined for the study case.

As can be noted in equations (12) and (13) the parameters of the I-P controller K_P and K_I depend on the location of the pole p_1, which in turn bounds the value of the pole p_2. The pole p_1 determines the time response of the control loop for the reference $\bar{\omega}^*_{fw}$. This time response can be very slow since the dynamics of $\bar{\omega}^*_{fw}$ depends on the average value of P_{wt}. Thus, the pole p_1 is set to $p_1 = 0.01$ rad/s. This implies a time response of the control loop system of 628 seconds approximately.

The value of K_I also depends on the parameter δ_{max} (see equation (8)). As a reminder, this parameters is given at maximum power developed by the flywheel P_{max} and at minimum operating rotational speed ω_{fw}. The maximum power is given by the maximum torque developed by the flywheel (12.2 Nm). Accordingly, the limit of the time varying parameter results $\delta_{max} = 0.122$ W/(rad/s)^2, assuming a minimum flywheel speed of 100 rad/s. Then, from equation (12), the parameter K_2 becomes

$$K_I = p_1 \delta_{max} = 0.0012 \text{ W/(rad/s)}. \quad (14)$$

Finally, applying equation (13), the value of the parameter K_P is set to

$$K_P = 0.1307 \text{ W/(rad/s)}^2 \quad (15)$$

provided that $p_2 = K_P/(J{\cdot}K_1)$ and J is 0.868 kg·m^2.

Figure 9 presents the frequency responses of T and $T_{d^*\omega}$ corresponding to the previous designed values of K_I and K_P. As can be noted, the closed loop system will be able to track speed references until the cutoff frequency of 0.01 rad/s, which corresponds to the location of the pole p_1. The frequency response of $T_{d^*\omega}$ shows that the infinity norm is below the limit $(\delta_{max})^{-1} = 8.19$ Nm/(rad/s) (18.3 dB). The graph also shows that the system is able to track torque references in the ranging from 0.01 to 0.1 rad/s with the maximum gain allowed by the stability guarantee and the flywheel torque limits.

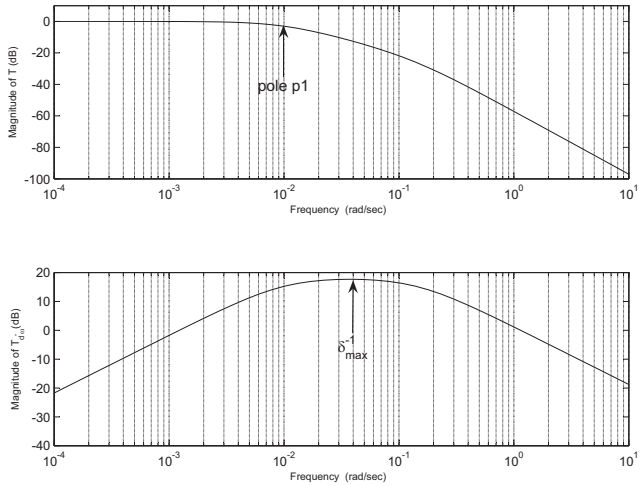

Fig. 9. Bode diagrams of the closed loop transfer function T (from $\bar{\omega}^*_{fw}$ to ω_{fw}) and the transfer function $T_{d^*\omega}$ (from d^* to ω_{fw}).

D. Analysis of the experimental results

Following contents present the obtained experimental results to evaluate the performance of the proposed energy management algorithm of the flywheel. As noted in previous sections, the wind turbine emulator reproduces the fluctuating power components depicted in Figure 8, that the flywheel test bench is in charge of compensating. Accordingly, Figure 10 depicts the actual power developed by the wind turbine emulator, the flywheel and the net power exchanged with the network.

As can be noted, the flywheel compensates the fluctuating components of wind power, leaving the net power profile almost constant. However, the average value of the power of the flywheel and thus of the net power exchanged with the network is not zero due to the necessity of compensating the power losses of the flywheel for maintaining the indicated average rotational speed $\bar{\omega}^*_{fw}$. The optimal average rotational speed is close to 220 rad/s in this case [26]. As this setup is meant to be a proof of concept system, the losses in the flywheel test bench are much higher than in a commercial flywheel storage device. In particular, the energy efficiency of the test bench is 73%, and the power losses depends on the rotational speed, reaching up to 800 W at rated speed [27]. These figures are far from those corresponding to a high-tech flywheel, in which the energy efficiency is around 90% and the power losses level at rated speed represents just 2% of the rated power [31].

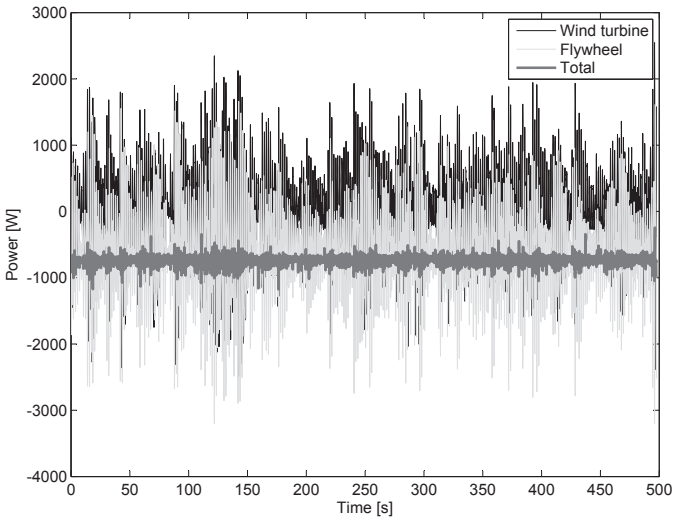

Fig. 10. Power of the wind turbine emulator, the flywheel and the net power exchanged with the network. The average rotational speed of the flywheel is $\bar{\omega}_{fw} = 220$rad/s.

Figure 11 examines more closely the previously presented power profiles in Figure 10. The power profile of the flywheel and the profile of the net power exchanged with the network have been corrected by subtracting the standing losses of the flywheel at the constant speed of $\bar{\omega}_{fw} = 220$ rad/s. This way, the average value of the power exchanged with the network and the average power profile of the flywheel are zero. As a result, in this Figure 11 it can be better observed that the instantaneous power of the flywheel compensates to a great extent the fluctuating components of the power of the wind turbine. This instantaneous regulation of the power of the flywheel is governed by the torque reference d^* (see Figure 3).

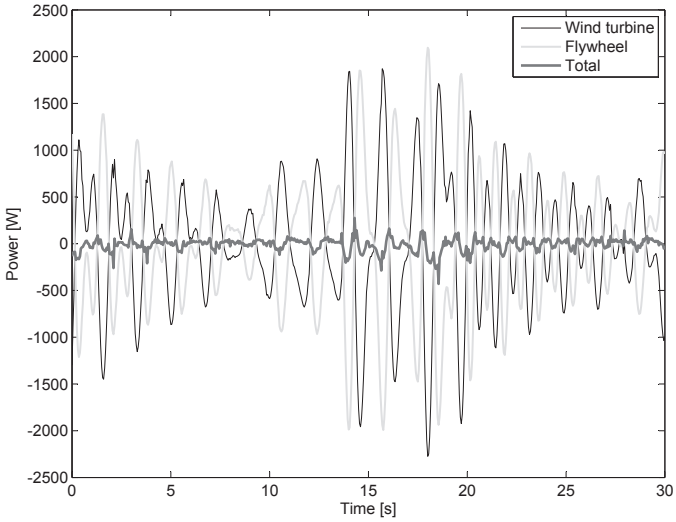

Fig. 11. Instantaneous power of the wind turbine emulator, as well as the power profiles of the flywheel and at the network terminals subtracting the standing losses of the flywheel. The average rotational speed of the flywheel is 220 rad/s.

The RMS currents of the flywheel, the wind turbine emulator and the network are depicted in Figure 12. As shown,

the magnitude of the currents of the flywheel are much higher than the currents of the wind turbine emulator, due to the necessity of compensating the losses of the system, as previously discussed. Without the proper losses compensation, the storage device will become completely discharged.

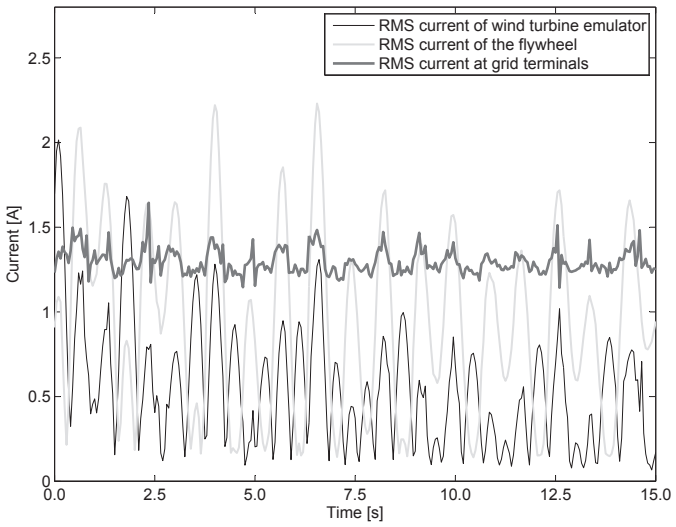

Fig. 12. RMS electrical currents of the wind turbine emulator, the flywheel and the network. The average rotational speed of the flywheel is $\bar{\omega}^*_{fw} = 220$ rad/s.

The spectrum of the power of the wind turbine emulator, as well as the total power exchanged with the network in case of considering the support of the flywheel are depicted in Figure 13. The average rotational speeds of the flywheel are 120 rad/s and 220 rad/s. As can be noted, the wind turbine emulator clearly represents the rotational sampling effect of the turbine at 0.6 and 1.2 Hz approximately. The rotating sampling effect is mostly compensated with the flywheel support. The constant component of the power spectrum of the flywheel due to its losses has been subtracted so that the performance of the system can be better observed. This figure depicts the support of the flywheel considering different average SoC. It is worth noting that the support that the flywheel can provide is better while rotating at 220 rad/s in average (close to the optimum) than while rotating at 120 rad/s. This is because the power capability of the flywheel is bounded by the product of the speed and the rated torque of the electrical machine and thus, as discussed in [26], there is an average optimal speed of the flywheel $\bar{\omega}^*_{fw}$ dependent on the magnitude of the fluctuating components of wind power to be compensated.

The performance of the system considering different flywheel average operating rotational speeds, is quantified from the attenuation of the fluctuating components of the net power exchanged with the network. This magnitude is computed from the data shown in Figure 13. The ratio between the energy of the fluctuating components of the net power exchanged with the network considering the flywheel support, and the fluctuating components of the wind turbine emulator, gives the attenuation. It is found an attenuation of 85% while the flywheel is rotating at 120 rad/s in average. The attenuation reaches the 92% with 220 rad/s as the average rotational speed of the flywheel.

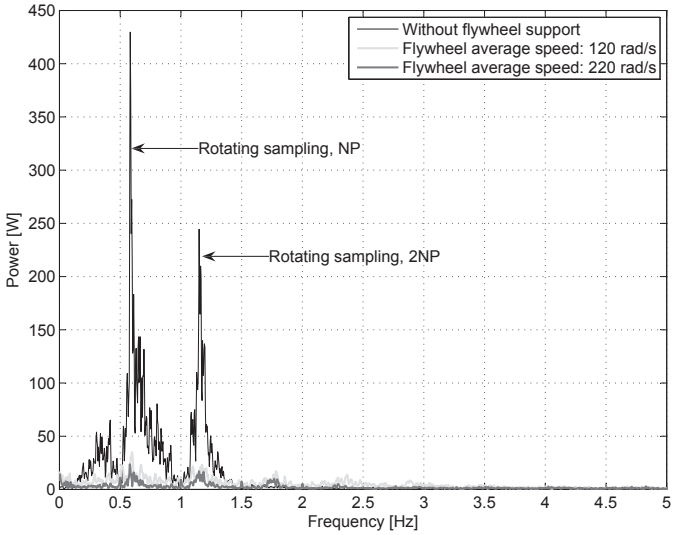

Fig. 13. Spectrum of the net power exchanged with the network without flywheel support, as well as with flywheel at different average SoC. The average power losses of the flywheel have been subtracted.

Apart from compensating the fast fluctuations of wind power, the second objective of the control system of the flywheel is to maintain a determined average rotational speed $\bar{\omega}^*_{fw}$. In regard of this experimental validation, some results are shown in the following. Figure 14 depicts the response of the flywheel to a step-profiled average speed reference $\bar{\omega}^*_{fw}$ from 220 rad/s to 270 rad/s. As shown, the time response is around 600 seconds, as imposed by the design of the controller presented in Section IV-C. Moreover, in the subplot below it can be observed that the voltage of the dc-link of the flywheel test bench keeps stable at 750 V in average, while regulating the rotational speed of the flywheel and compensating the fast wind power fluctuations.

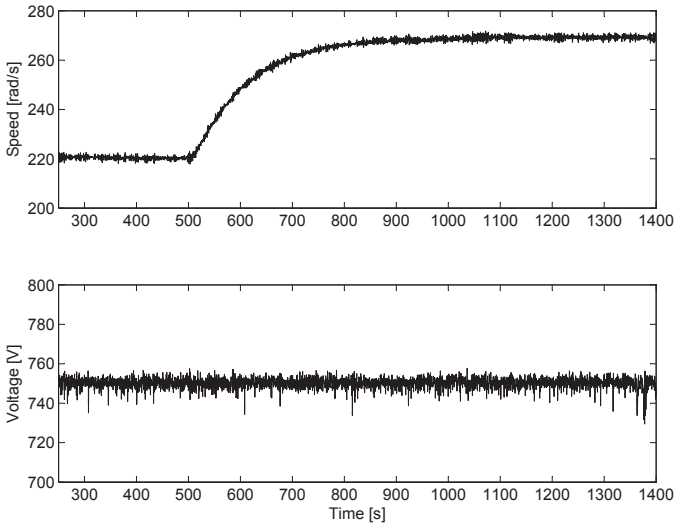

Fig. 14. Rotational speed of the flywheel in response to a step-profiled average speed reference $\bar{\omega}^*_{fw}$ from 220 rad/s to 270 rad/s. The dc-link voltage of the flywheel test bench is presented in the bottom subplot.

As indicated in Section IV-B, in previous experiments the fluctuating components of wind power to be compensated by

the flywheel are emulated, and not the whole spectrum of it. This is carried out with the aim of adjusting the magnitude of these fluctuating power components to the ratings of the wind power emulator and the flywheel test bench. However, in the following concluding experimental results, the whole spectrum of wind power is emulated instead. The resultant of the low-pass filtering of this signal, $\bar{P}_{wt}$, serves as an input to a $P-\omega$ droop characteristic, as depicted in Figure 3. This droop characteristic determines, in turn, a changing average speed reference $\bar{\omega}^*_{fw}$ for the flywheel depending on the value of $\bar{P}_{wt}$. The results of this experiment, which are depicted in Figure 15, complement the performance evaluation of the control loop in charge of the tracking of the average speed reference $\bar{\omega}^*_{fw}$.

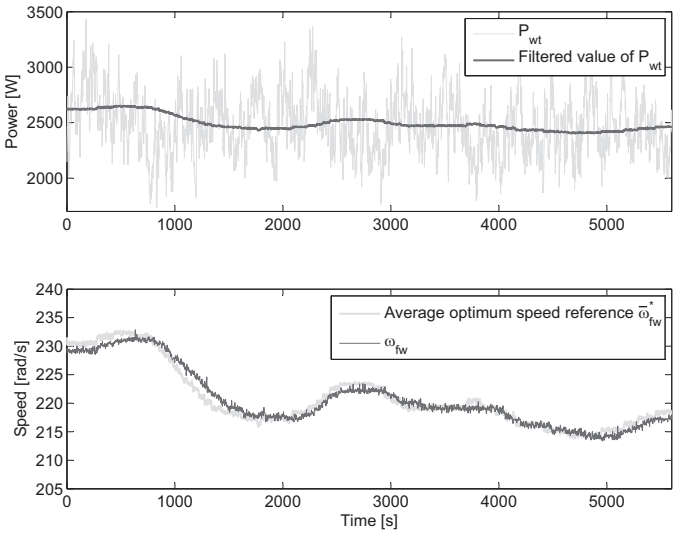

Fig. 15. Wind power emulation and the resultant of its low pass filtering, $\bar{P}_{wt}$, presented in the upper subplot. In the subplot below, the corresponding $\bar{\omega}^*_{fw}$ to $\bar{P}_{wt}$ determined by the $P-\omega$ droop characteristic is presented. The tracking of the speed reference $\bar{\omega}^*_{fw}$ by the flywheel is also depicted.

The wind power profile is presented in Figure 15, upper subplot. This represents the power of a 1.5 MW wind turbine with a scaling factor of 200. Moreover, the resultant of its low pass filtering $\bar{P}_{wt}$, which is computed by the DSP of the control board of the machine side power converter of the flywheel, is also indicated. The mathematical expression of the filter is included in the Appendix. The varying average trend of the wind power profile $\bar{P}_{wt}$ has been achieved from imposing a varying average trend in the wind. These wind data have been extracted from the NREL's online database for wind speeds [33].

Figure 15, subplot below, depicts the speed measurement of the flywheel, and the reference $\bar{\omega}^*_{fw}$ determined by the $P-\omega$ droop characteristic. Using this droop characteristic, the signal $\bar{\omega}^*_{fw}$ is varied linearly from 150 rad/s, considering an average wind power $\bar{P}_{wt}$ of 1500 W, to 300 rad/s, with $\bar{P}_{wt}$ of 3500 W. This leads noticeable variations of $\bar{\omega}^*_{fw}$, which are preferable for the purposes of the experiment. As can be noted, the designed feedback control successes in the tracking of the reference $\bar{\omega}^*_{fw}$.

V. Conclusions

A high-level energy management algorithm of a flywheel for power smoothing in wind generation systems has been designed. The algorithm is based on feedback control techniques. The controller has been conveniently formulated and tuned so that the robustness as well as the desired time response of the storage device can be ensured. The algorithm successes in letting the flywheel maintain an optimum average rotational speed while enabling the fast accelerations and decelerations of the storage device for smoothing the fast fluctuating components of the power of the wind turbine. The maintenance of the indicated average rotational speed of the flywheel avoids the progressive discharge of the storage device in its operation. Also, the control capability of the average rotational speed of the flywheel, permits to adjust the average SoC of the storage device to the magnitude of the power and energy to exchange. The controller has been validated experimentally in scale-lab equipments. Results show that most of the fluctuating components of the power of the wind turbine due to the rotating sampling effect can be compensated through the flywheel support.

This article proves that the short time response and high controllability define flywheel systems as well suited devices to compensate the variability of the power generated by wind turbines and thus, to promote their integration into the network. The quality of the power injected into the grid by a wind turbine or by a wind power plant, can be improved by adding a flywheel-based energy storage system to the generating facility.

VI. Acknowledgments

This work was supported by KIC InnoEnergy SE under the project Smart Power and the Ministerio de Economía y Competitividad, Plan Nacional de I+D+i under Project ENE2012-33043.

VII. Appendix

A. Characteristic parameters of the experimental setup

The characteristic parameters of the system are presented in Table I.

B. Filter's design

The fluctuating components of the wind turbine power profile P_{fluc} are identified through the application of a third order high pass filter (Butterworth type) to the wind power profile P_{wt}. The cutoff frequency of the filter is 0.4 Hz and the sampling period 20 ms. Its mathematical expression is

$$F_H(z) = \frac{1 - 2.9975z^{-1} + 2.9951z^{-2} - 0.9976z^{-3}}{1 - 2.8995z^{-1} + 2.8040z^{-2} - 0.9044z^{-3}}. \quad (16)$$

Moreover, the average wind power $\bar{P}_{wt}$ is identified through the application of a second order low pass Butterworth filter to the wind power profile P_{wt}. The cutoff frequency is 0.0003 Hz and the sampling period 5 s. The mathematical expression is

$$F_L(z) = 10^{-4}\frac{0.5456z^{-1} + 0.5429z^{-2}}{1 - 1.9852z^{-1} + 0.9853z^{-2}}. \quad (17)$$

TABLE I
CHARACTERISTIC PARAMETERS OF THE SYSTEM

System	Parameter	Value
Wind turbine emulator	2 3-phase IGBT bridge in back-to-back	
	S_{rated} (kVA)	4.0
	$U_{ACrated}$ (V)	400.0
	$U_{DCrated}$ (V)	750.0
	I_{max} (A)	16.0
	C (F)	0.005
Flywheel	Ratings	3.0 kW @ 30 kWs
	Efficiency	73%
	ω_{max} (rpm)	3000.0
	ω_{min} (rpm)	1000.0
	T_{rated} (Nm)	12.2
	J (kg·m^2)	0.868
Flywheel (PMSM)	ψ_m (Wb)	0.2465
	L_d & L_q (H)	$2.88{\cdot}10^{-3}$
	R_s (Ω)	0.44
	pole pairs	2
Flywheel (power electronics)	(same as emulator)	

REFERENCES

[1] Muljadi E, Butterfield CP, Chacon J, Romanowitz H. Power quality aspects in a wind power plant. In: IEEE Power Engineering Society General Meeting 2006;1-10

[2] Hu W, Chen Z, Wang Y, Wang Z. Flicker mitigation by active power control of variable-speed wind turbines with full-scale back-to-back power converters. IEEE Transactions on Energy Conversion 2009;24:640-649

[3] Sørensen P, Hansen AD, Carvalho-Rosas PA. Wind models for simulation of power fluctuations from wind farms. Journal of Wind Engineering and Industrial Aerodynamics 2002;90:1381-1402

[4] Bianchi FD, De Batista H, Mantz RJ. Wind turbine control systems. Principles, modeling and gain scheduling design. Springer; 2007

[5] Tascikaraoglu A, Uzunoglu M, Vural B, Erdinc O. Power quality assessment of wind turbines and comparison with conventional legal regulations: A case study in Turkey. Applied Energy 2011;88:1864-1872

[6] Sebastián R, Peña Alzola, R. Flywheel energy storage systems: Review and simulation for an isolated wind power system. Renewable and Sustainable Energy Reviews 2012;16:6803-6813

[7] Díaz-González F, Sumper A, Gomis-Bellmunt O, Villafáfila-Robles R. A review of energy storage technologies for wind power applications. Renewable and Sustainable Energy Reviews 2012;16:2154-2171

[8] Ribeiro PF, Johnson BK, Crow ML, Arsoy A, Liu Y. Energy storage systems for advanced power applications. Proceedings of the IEEE 2001;89:1744-1756

[9] Zafirakis D, Chalvatzis KJ, Baiocchi G, Daskalakis G. Modeling of financial incentives for investments in energy storage systems that promote the large-scale integration of wind energy. Applied Energy 2013;105:138-154

[10] Liu H, Jiang J. Flywheel energy storage - an upswing technology for energy sustainability. Energy and Buildings 2007;39:599-604

[11] Yogi-Goswami D, Kreith F. Energy conversion. CRC Press Taylor & Francis Group; 2007

[12] Bolund B, Bernhoff H, Leijon M. Flywheel energy and power storage systems. Renewable & Sustainable Energy Reviews 2007;11:235-58

[13] Dai X, Deng Z, Liu G, Tang X, Zhang F, Deng Z. Review on advanced flywheel energy storage system with large scale. Transactions of China Electrotechnical Society 2011;26:133-40

[14] Hadjipaschalis I, Poullikkas A, Efthimiou V. Overview of current and future energy storage technologies for electric power applications. Renewable and Sustainable Energy Reviews 2009;13:1513-22

[15] Boukettaya G, Krichen L, Ouali A. A comparative study of three different sensorless vector control strategies for a Flywheel Energy Storage System. Energy 2010;35:132-9

[16] Cardenas R, Peña R, Asher G, Clare J, Blasco-Giménez R. Control strategies for power smoothing using a flywheel driven by a sensorless vector-controlled induction machine operating in a wide speed range. IEEE Transactions on Industrial Electronics 2004;51:603-614

[17] Ghedamsi K, Aouzellag D. Improvement of the performances for wind energy conversions systems. Electrical Power and Energy Systems 2010;32:936-945

[18] Cardenas R, Peña R, Pérez M, Clare J, Asher G, Wheeler P. Power smoothing using a flywheel driven by a switched reluctance machine. IEEE Transactions on Industrial Electronics 2006;53:1086-1093

[19] Cardenas R, Peña R, Asher G, Clare J. Control strategies for enhanced power smoothing in wind energy systems using a flywheel driven by a vector-controlled induction machine. IEEE Transactions on Industrial Electronics 2001;48:625-635

[20] Jerbi L, Krichen L, Ouali A. A fuzzy logic supervisor for active and reactive power control of a variable speed wind energy conversion system associated to a flywheel storage system. Electric Power Systems Research 2009;79:919-925

[21] Cimuca GO, Saudemont C, Robyns B, Radulescu MM. Control and performance evaluation of a flywheel energy-storage system associated to a variable-speed wind generator. IEEE Transactions on Industrial Electronics 2006;53:1074-1085

[22] Leclercq L, Robyns B, Grave J-M. Control based on fuzzy logic of a flywheel energy storage system associated with wind and diesel generators. Mathematics and Computers in Simulation 2003;63:271-280

[23] Jun-Keun J. DSP-based self-tuning IP speed controller with load torque compensation for rolling mill DC drive. IEEE Transactions on Industrial Electronics 1995;42:282-386

[24] Mohamed YA-RI. Adaptive self-tuning speed control for permanent-magnet synchronous motor drive with dead time. IEEE Transactions on Energy Conversion 2006;21:855-862

[25] de Prada-Gil M, Gomis-Bellmunt O, Sumper A, Bergas-Jané J. Power generation efficiency analysis of offshore wind farms connected to a SLPC (single large power converter) operated with variable frequencies considering wake effects. Energy 2012;37:455-468

[26] Díaz-González F, Sumper A, Gomis-Bellmunt O, Bianchi F.D. Energy management of flywheel-based energy storage device for wind power smoothing. Applied Energy 2013;110:207-219

[27] Díaz-González F, Sumper A, Gomis-Bellmunt O, Villafáfila-Robles R. Modeling, control and experimental validation of a flywheel-based energy storage device. Journal of European Power Electronics 2013;23

[28] Ruiz-Álvarez A, Colet-Subirachs A, Álvarez-Cuevas F, Gomis-Bellmunt O, Sudria-Andreu A. Operation of a utility connected microgrid using an IEC 61850-based multi-level management system. IEEE Transactions on Smart Grid 2012;3:858-865

[29] P. C. Krause, O. Wasynczuk, and S. D. Sudhoff. Analysis of electric machinery and drive systems. New York, Wiley, 2002.

[30] G. Terorde. Electrical drives and control techniques. Leuven, Acco, 2004.

[31] M. Lazarewicz. Status of flywheel storage operation of first frequency regulation plants. Beacon Power Corporation, 2011.

[32] S. Skogestad, and I. Postlethwaite. Multivariable feedback control, analysis and design. Chichester, John Wiley and Sons Ltd., 2007

[33] National Renewable Energy Laboratory webpage: *http://www.nrel.gov/*. Access data: 24/09/2013